Cytokine signaling converging on IL11 in ILD fibroblasts provokes aberrant epithelial differentiation signatures

Miriam T. Kastlmeier[1], Erika Gonzalez Rodriguez[1], Phoebe Cabanis[1], Eva M. Guenther[1], Ann-Christine König[2], Lianyong Han[1], Stefanie Hauck[2], Tobias Stoeger[1], Anne Hilgendorff[1,3]*, and Carola Voss[1]*

[1]Institute of Lung Health and Immunity, Comprehensive Pneumology Center Munich with the CPC-M bioArchive, Helmholtz Center Munich, Research Center for Environmental Health, Member of the German Center of Lung Research (DZL), Germany
[2]Metabolomics and Proteomics Core (MPC) Helmholtz Center Munich, Research Center for Environmental Health, Germany
[3]Dr. von Haunersche Children's Hospital, Hospital of the Ludwig-Maximilians University, Member of the German Lung Research Center (DZL), Munich, Germany

*** Correspondence:**
Carola Voss
carola.voss@helmholtz-muenchen.de

Anne Hilgendorff
anne.hilgendorff@med.uni-muenchen.de

Keywords: cytokine[1], IL11[2], secretome[3], interstitial lung disease[4], organoids[5], human pluripotent stem cells[6], disease modeling[7], co-culture model[8]

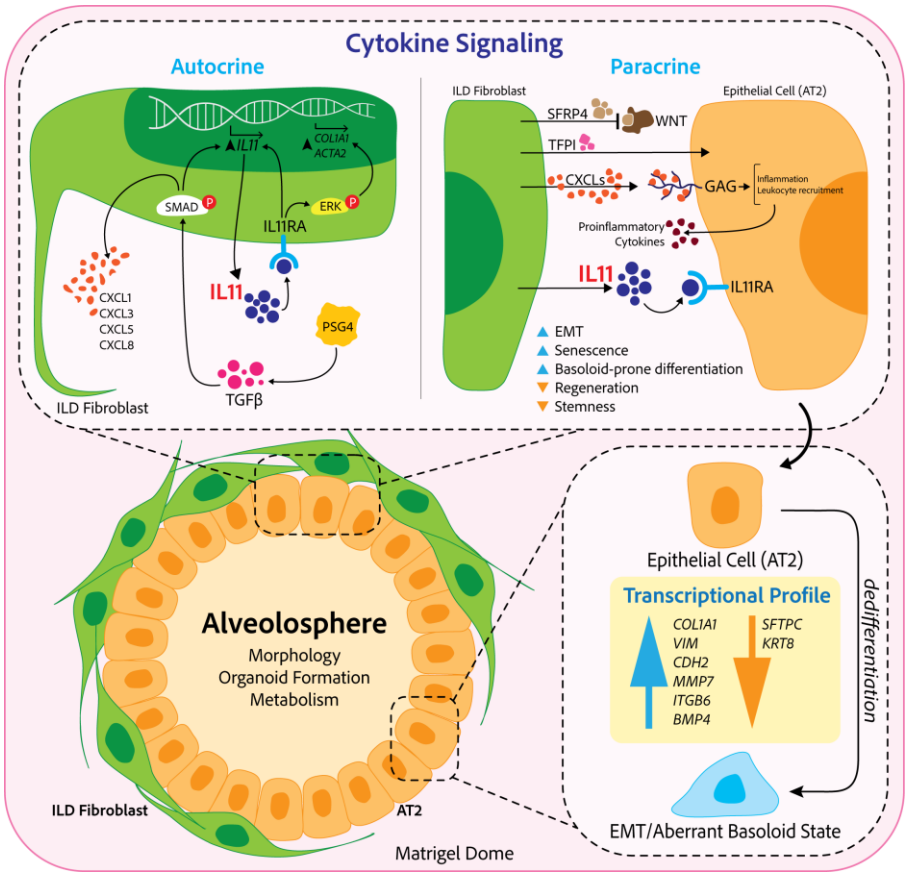

Abstract

Fibrotic interstitial lung disease (ILD) is a group of lung disorders characterized by the accumulation of extracellular matrix, ultimately resulting in the destruction of the pulmonary scaffold. Continuous mesenchyme-derived profibrotic signaling perpetuates the remodeling process, specifically targeting the epithelial cell compartment, thereby destroying the gas exchange area. Studies that address this detrimental crosstalk between lung epithelial cells and fibroblasts are key to understanding ILD.

With the aim of identifying functionally relevant targets that drive lung mesenchymal-epithelial crosstalk and their potential as new avenues to therapeutic strategies, we developed a 3D organoid co-culture system based on human induced pluripotent stem cell (hiPSC)-derived alveolar epithelial type 2 cells (iAT2s) and lung fibroblasts from ILD patients as well as IMR-90 controls. While organoid formation capacity and organoid size was comparable in the presence of ILD or control lung fibroblasts, metabolic activity was significantly increased in ILD co-cultures. Alveolar organoids cultured with ILD fibroblasts further demonstrated reduced stem cell function supported by reduced *Surfactant Protein C (SFTPC)* gene expression together with an aberrant basaloid-prone differentiation program indicated by elevated *Cadherin 2 (CDH2)*, *Bone Morphogenic Protein 4 (BMP4)* and *Vimentin (VIM)* transcription.

In order to identify key mediators of the misguided mesenchymal-to-epithelial crosstalk with a focus on disease-relevant inflammatory processes, we used secretome mass spectrometry to identify key signals secreted by end stage ILD lung fibroblasts. Over 2000 proteins were detected in a single-shot experiment with 47 differentially upregulated proteins when comparing ILD and non-Chronic Lung Disease (CLD) control fibroblasts.

The secretome profile was dominated by chemokines of the C-X-C motif family, including CXCL1, CXCL-3, and -8, all interfering with (epithelial) growth factor signaling orchestrated by Interleukin 11 (IL11), steering fibrogenic cell-cell communication, and proteins regulating extracellular matrix remodeling including epithelial-to-mesenchymal transition (EMT). When in turn treating 3D monocultures of iAT2s with IL11 we recapitulated the co-culture results obtained with primary ILD fibroblasts including changes in metabolic activity as well as organoid formation capacity and size.

In summary, our analysis identified mesenchyme-derived mediators likely contributing to the disease-perpetuating mesenchymal-to-epithelial crosstalk in ILD by using sophisticated alveolar organoid co-cultures indicating the importance of cytokine-driven aberrant epithelial differentiation and confirmed IL11 as a key player in ILD using an unbiased approach.

1 Introduction

Interstitial lung diseases (ILDs) comprise a variety of chronic pulmonary conditions that are characterized by structural remodeling of the gas exchange area (Glasser et al., 2010). ILD pathophysiology is centered on sustained inflammation and progressive scarring, ultimately resulting in organ failure. Despite the exact pathogenesis of ILD still being unclear, genetic predisposition, age, sex and environmental exposure are known drivers of the disease (Lederer & Martinez, 2018; Strikoudis et al., 2019).

Fibroblast activation occurs directly by exogenous stimuli and indirectly through the activation of innate immune cells, especially monocytes and neutrophils through transforming growth factor ß (TGF-β) and Interleukin 17 (IL17) secretion. Matrix metalloproteinases (MMPs), fibroblast growth factors and metabolic changes leading to lactic acid release from both, fibroblasts and epithelial cells furthermore drive fibroblast activation and accumulation (O'Dwyer et al., 2016). As a result, fibroblasts merge to fibroblastic foci, becoming the main loci of extracellular matrix (ECM) production and deposition. Further enhancing the pro-fibrotic circle of events, activated fibroblasts induce epithelial-to-mesenchymal transition (EMT) in alveolar epithelial cells (Kim et al., 2018) *via* SMAD and MAPK

signaling through repeated inflammatory epithelial injury leading to further leucocyte attraction and infiltration of the airspace and ultimately loss of the alveolar epithelium (O'Dwyer et al., 2016).
Disease progression is continuously upheld by the bidirectional cellular crosstalk between the activated fibroblast differentiation and the damaged epithelium (Ng et al., 2020; Ng et al., 2019; Yao et al., 2021). Amongst other players identified, TGF-β signaling holds a central role in the initiation and progression of pulmonary fibrosis. As a driver of the sustained pathological tissue remodeling processes that results in ECM expansion in ILD end stage pulmonary fibrosis, a tightly knit mesenchymal-to-epithelial crosstalk has been proposed highlighting the role of pathologic growth factor signaling and secreted cytokines. Next to inducing EMT, activated fibroblasts have been shown to alter AT2 stem cell potential (Mou, 2021).
To address knowledge gaps focusing on cytokine driven disease initiating mesenchymal-to-epithelial crosstalk, we used lung organoids derived from human induced pluripotent stem cells (hiPSCs) through chemical directed differentiation. hiPSC-derived alveolar type 2 cells (iAT2s, alveolospheres) are a useful tool to study lung diseases and regeneration, and are recently emerging as New Approach Methodology (NAM) in environmental and occupational hazard assessment (Kastlmeier et al., 2022; Kong et al., 2021). Additionally, alveolospheres recapitulate the characteristic three-dimensional structure of alveoli, holding important functions of the gas exchange area *in vitro*, wherefore they are a reliable source to study pulmonary disease (Hogan, 2021; Nikolić et al., 2018). Organoids are particularly versatile in studying underlying molecular mechanisms of disease *in vitro* (Strikoudis et al., 2019).
In this study we investigated the impact of primary ILD patient-derived lung fibroblast signaling on critical functions of hiPSC-derived alveolospheres by the use of a novel co-culture model in combination with unbiased secretome analysis to delineate key signals of the pathophysiological crosstalk from mesenchyme towards the alveolar epithelium with functional relevance for disease progression.

2 Material and Methods

2.1 Human induced pluripotent stem cells (hiPSCs) and directed differentiation into lung progenitors

The hiPSC line BU3NGST was kindly provided by Prof. Darrell Kotton, Boston University, Center for Regenerative Medicine. This cell line is a dual-reporter construct composed of fluorochrome-encoding cassettes targeted to the endogenous NKX2.1 and SFTPC loci (BU3 NKX2.1^{GFP}; SFTPC^{tdTomato}) (Hawkins et al., 2017). hiPSCs were maintained in mTeSR1 (StemCell Technologies), on Matrigel (Corning) coated cell culture plates at 37 °C/5 % CO_2 in a cell culture CO_2 incubator. Cells were passaged by using ReLeSR (StemCell Technologies) or Gentle Cell Dissociation Reagent (StemCell Technologies) (Jacob et al., 2017; Jacob et al., 2019).
BU3NGSTs were differentiated into NKX2.1^{+} lung progenitor cells and iAT2s as described previously by Jacob et al. (Jacob et al., 2019). hiPSCs were checked for their pluripotency *via* Alkaline Phosphatase staining (ES Cell Characterization Kit, CHEMICON International) or immunofluorescence staining of TRA 181 and SSEA 4 (ES cell characterization Kit, CHEMICON International). Induction of definitive endoderm was conducted *via* STEMdiff Definitive Endoderm Kit, (StemCell Technologies). On day 14 of differentiation, lung progenitor specification was evaluated by immunofluorescence staining of NKX2.1 (Invitrogen) and Albumin (ALB, R&D Systems). NKX2.1^{GFP+} lung progenitor cells were enriched by GFP signal for NKX2.1 based on a previously described protocol. The sorting was performed by FACS cell sorting at MACSQuant Tyto Cell Sorter (Miltenyi Biotec). For data evaluation FlowJo Version 7.2.1 and v10 was used. Purified lung

progenitors were seeded in Matrigel (Corning) domes at a cell density of 50 cells/µL and passaged every second week according to published protocols. To increase SFTPC$^{tdTomato+}$ cells CHIR withdrawal and addback was performed according to published protocols. At day 45 of differentiation, iAT2s were enriched by flow cytometry (MACSQuant Tyto Cell Sorter, Miltenyi Biotec) using tdTomato signal for SFTPC expression and subsequently cultured as 3D alveolospheres. Differentiated SFTPC$^{tdTomato+}$ iAT2 cells in 3D Matrigel were grown in CK+DCI medium, with media changes every 48 - 72 h. Alveolospheres were passaged every 14 days.

2.2 Primary human fibroblast culture

Human fetal lung fibroblasts (IMR-90, P8) for control co-cultures were obtained from ATCC (Catalog # CCL-186™) and grown in Dulbecco's Modified Eagle Medium: Nutrient F-12 (DMEM/F12; Gibco) with 20 % fetal bovine serum (FBS SUPERIOR, Sigma) and 1 % penicillin-streptomycin (Pen Strep, Gibco). Cultured primary human lung fibroblasts from ILD patients and non-CLD controls (P4) for secretome analysis, were seeded in 6-well plates. Cells were seeded at a density of $1x10^5$ cells in 2 mL media (DMEM/F12, 20 % FBS, 1 % penicillin/streptomycin) per well of a 6-well plate until reaching 80 % confluency. Once confluent, each well was washed three times with a 15-minute incubation per wash with 1 mL of FBS-free culturing medium (DMEM/F12, 1 % penicillin/streptomycin) to eliminate remaining FBS. Fibroblasts were cultured for 48 h in FBS-free medium, supernatants were collected and stored at -80 °C for further analysis.
Primary human fibroblasts were isolated according to published protocol (Heinzelmann et al., 2018) and obtained through the CPC-M bioArchive at the Comprehensive Pneumology Center in Munich, Germany. The study was approved by the local ethics committee of the Ludwig-Maximilians University of Munich, Germany (Ethic vote #333-10). Written informed consent was obtained for all study participants.

2.3 Secretome analysis by mass spectrometry

<u>Sample preparation for proteomics</u>
Each 500µL supernatant was subjected to tryptic digest applying a modified filter aided sample preparation (FASP) procedure (Grosche et al. 2015; Wiśniewski et al. 2009). After protein reduction and alkylation using DTT and iodoacetamide, samples were denatured in UA buffer (8 M urea in 0.1 M Tris/HCl pH 8.5) and centrifuged on a 30 kDa cut-off filter device (PALL or Sartorius) and washed thrice with UA buffer and twice with 50 mM ammoniumbicarbonate (ABC). Proteins were proteolysed for 2 h at room temperature using 0.5 µg Lys-C (Wako) and subsequently for 16 h at 37 °C using 1 µg trypsin (Promega). Peptides were collected by centrifugation and acidified with 0.5 % trifluoroacetic acid (TFA).

<u>Mass spectrometric measurements</u>
LC-MSMS analysis was performed on a Q-Exactive HF mass spectrometer (Thermo Scientific) each online coupled to a nano-RSLC (Ultimate 3000 RSLC; Dionex). For subsequent analysis on the Q-Exactive HF, tryptic peptides were accumulated on a nano trap column (300 µm inner diameter × 5 mm, packed with Acclaim PepMap100 C18, 5 µm, 100 Å; LC Packings) and then separated by reversed phase chromatography (nanoEase MZ HSS T3 Column, 100Å, 1.8 µm, 75 µm X 250 mm; Waters) in a 80 minutes non-linear gradient from 3 to 40 % acetonitrile (ACN) in 0.1 % formic acid (FA) at a flow rate of 250 nL/min. Eluted peptides were analyzed by the Q-Exactive HF mass spectrometer equipped with a PepSep PSS1 source. Full scan MS spectra (from m/z 300 to 1500) and MSMS fragment spectra were acquired in the Orbitrap with a resolution of 60,000 or 15000 respectively, with maximum injection times of 50 ms each. The up to ten most intense ions were

selected for HCD fragmentation depending on signal intensity (TOP10 method). Target peptides already selected for MS/MS were dynamically excluded for 30 seconds.

Protein Identification and label-free quantification

Proteome Discoverer 2.5 software (Thermo Fisher Scientific; version 2.5.0.400) was used for peptide and protein identification via a database search (Sequest HT search engine, SequestHT score:1) against Swissprot human data base (Release 2020_02, 20432 sequences), considering full tryptic specificity, allowing for up to two missed tryptic cleavage sites, precursor mass tolerance 10 ppm, fragment mass tolerance 0.02 Da. Carbamidomethylation of Cys was set as a static modification. Dynamic modifications included deamidation of Asn, Gln and Arg, oxidation of Pro and Met; and a combination of Met loss with acetylation on protein N-terminus. Percolator was used for validating peptide spectrum matches and peptides, accepting only the top-scoring hit for each spectrum, and satisfying the cutoff values for FDR <5%, and posterior error probability <0.01.

The quantification of proteins was based on abundance values for unique peptides. Abundance values were normalized on total peptide amount and protein abundances were calculated summing up the abundance values for admissible peptides. The final protein ratio was calculated using median abundance values. The statistical significance of the ratio change was ascertained employing the T-test approach described in Navarro et al., 2014 (Navarro et al., 2014), which is based on the presumption that we look for expression changes for proteins that are just a few in comparison to the number of total proteins being quantified. The quantification variability of the non-changing "background" proteins can be used to infer which proteins change their expression in a statistically significant manner. Proteins considered to be up- or downregulated were filtered with the following criteria: proteins were considered to be downregulated below an abundance of ratio of 0.5 and upregulated above 2, proteins identified with a single peptide were excluded and just significant proteins were considered (P value < 0.05, P values were adjusted for multiple testing by Benjamini-Hochberg correction). Additionally, at least two MSMS identifications had to be identified to include the protein ratio.

Enrichment analysis

Pathway enrichment analysis were performed in Cytoscape (3.9.0) with the ClueGo plugin (v2.5.8) for significant up- and downregulated proteins. The following ontologies were used: KEGG (8093), GO_MolecularFunction-EBI-UniProt (18336), GO_BiologicalProcess-EBI-UniProt (18058). Accession IDs were used as identifiers and the analysis was performed with the standard software settings provided in the ClueGo app (Bindea et al., 2009).

2.4 Mesenchymal-epithelial co-culture

Primary lung ILD fibroblasts and IMR-90 (control fibroblast cell line) were grown in cell culture flasks until 70 % confluent. A single cell suspension was prepared using 0.25 % EDTA-Trypsin (Gibco). iAT2s were grown for up to two weeks in Matrigel domes. Single cell suspension was obtained with Dispase (Corning) and 0.25 % EDTA-Trypsin as described by Jacob et al. (Jacob et al., 2019). Human ILD/IMR-90 control fibroblasts and iAT2s were counted and directly seeded either in equal seeding densities 1:1 (F_{low}) or 1:5 (F_{high}) (iAT2s to fibroblasts) in undiluted Matrigel domes in 8-chamber wells (20 µL Drops, Falcon), 96-well plates (50 µL Drops, Greiner) or 12-Well plates (50 µL Drops, Greiner). Co-cultures were cultured in CK+DCI media and media was changed every 48 h to 72 h, for up to 12 days of cultivation.

2.5 Immunofluorescence microscopy

3D alveolospheres and co-cultures cultured in 8-chamber wells (Nunc Lab-Tek Chamber Slide System, 8 wells, Permanox slide, 0.8 cm^2/well) were fixed with ice cold methanol and acetone (1:1v/v) for 5 minutes at -20 °C. Cells were washed with PBS and stained with the respective primary antibody in buffer containing 0.1 % BSA and 0.1 % Triton X-100 overnight at 4 °C. The next day, cells were washed 3 times with PBS and incubated in buffer with the respective fluorescent conjugated secondary antibody at a dilution of 1:500 and DAPI diluted 1:1.000 overnight at 4 °C. The following day, cells were washed gently, growth camber removed and remaining microscope slide mounted with fluorescent mounting media (Dako) and covered with a coverslip. Slides were stored at 4 °C until imaging. Imaging was performed using a confocal laser scanning microscope (CLSM) Zeiss LSM 880 with Airyscan and edited afterwards using ZEN 2.5 software (Zeiss). Detailed information on the primary and secondary antibodies are given in Supplementary Table 1.

2.6 Operetta high content imaging

Live imaging of all hiPSC co-cultures was performed using the Operetta CLS high-content analysis system (Operetta CLS, PerkinElmer) at time points 5, 8 and 12 days during the co-culture experimental set-up. Pictures were analyzed by the Harmony 3.5.2 high-content imaging and analysis software with PhenoLOGIC. Through the Napari image viewer (Python) maximum intensity projections of 3D images were appointed and growing pattern and organoid formation capacity between iAT2 cells and human fibroblasts (control or ILD) could be determined.

2.7 Quantitative real-time PCR

Co-cultures were lysed in RLT Plus Lysis Buffer (Qiagen) and RNA isolation was performed with the RNeasy Mini Kit (Qiagen) according to the manufacturer's instructions. Cell lysis from organoids and co-culture assays was performed with peqGOLD TriFast (VWR Life Science) as recommended by the manufactures followed by RNA isolation with the RNeasy Mini Kit (Qiagen). RNA was transcribed into cDNA by reverse transcriptase using the High-Capacity cDNA Reverse Transcription Kit (Thermo Fisher Scientific) according to the manufacturer's instructions. 5 ng of cDNA was added to a final concentration volume of 10 µL, Random Nonamers (Metabion) and master mix (Invitrogen, Thermo Fisher Scientific) was added to each RNA sample. cDNA was diluted with ultrapure H_2O. qPCR was performed in 96-well format using the quantitative real-time PCR System (Roche 480 LightCycler). 2 µL cDNA were added to a final reaction volume of 10 µL containing H_2O, 480 SYBR Green (LightCycler, Roche Diagnostics) and the primer mix (100 µM). Gene expression was normalized to ß-Actin control for genes *Vimentin* (*VIM*), *Integrin Subunit Beta 6* (*ITGB6*) and *Cadherin 2* (*CDH2*), and normalized to an average of ß-Actin and HRPT control for genes *Surfactant Protein C* (*SFTPC*), *Keratin 8* (*KRT8*), *Collagen 1A1* (*Col1A1*), *Matrix Metallopeptidase* (*MMP7*) and *Bone Morphogenic Protein* 4 (*BMP4*), the fold change was calculated using the 2^ (-ddC) method. Sequence information of used primers are given in Supplementary Table 2. Data obtained from qPCR are presented relative to respective control co-cultures, to demonstrate influence of disease background. Original data with relative expression to housekeeping genes are shown in Supplementary Figure 2.

2.8 Metabolic activity estimated by WST-1 assay

The WST-1 assay for cell proliferation and viability was performed at day 2, 3, 5 and 7 of the co-cultures containing iAT2s and human ILD and IMR-90 control fibroblasts. Cell proliferation reagent WST-1 (Roche Diagnostics) was added to the culture medium in a 1:10 dilution. The culture medium was used as background control. After 2 h of incubation at 37 °C and 5 % CO_2, 100 µL of media from every sample was transferred to a microplate (Thermo Scientific; Fisher Scientific) and the absorbance

of the sample against the background was measured with a TECAN reader (TECAN; infinite M200 PRO).

3 Results

3.1 ILD fibroblasts induce changes in morphology and metabolic activity of iAT2s

Successful co-culture of iAT2 with both ILD or IMR-90 control fibroblasts (experimental workflow in Figure 1A) resulted in the robust formation of proliferative organoids. Cell-cell contact of iAT2s with ILD fibroblast in co-culture was shown by partial encapsulation of epithelial organoids by a α-SMA expressing fibroblast (Figure 1B, white arrows).

High-resolution images of the 3D co-cultures revealed changes to organoid formation capacity and morphology induced by the seeding ratios, i.e. iAT2 to fibroblast number, independent of disease (Figure 1C). Here, quantitative assessment of organoid area and number of high content images obtained from all four co-culture conditions (Figure 1C, D, E) demonstrated a reduced capacity for iAT2s to form organoids with increasing fibroblast seeding numbers (ILD and IMR-90). At the same time, alveolospheres formed bigger organoids when grown in presence of those fibroblasts and lose their circular appearance compared with alveolosphere monocultures (Figure 1C, D).

In contrast to the seeding ratio dependent findings, ILD fibroblasts provoked reduction in organoid size when seeded in high density as compared to control IMR-90 fibroblasts (Figure 1E). Further, ILD fibroblasts led to increased metabolic activity as assessed by WST-1 assay in iAT2 organoids in comparison to IMR-90 control cells (Figure 1F).

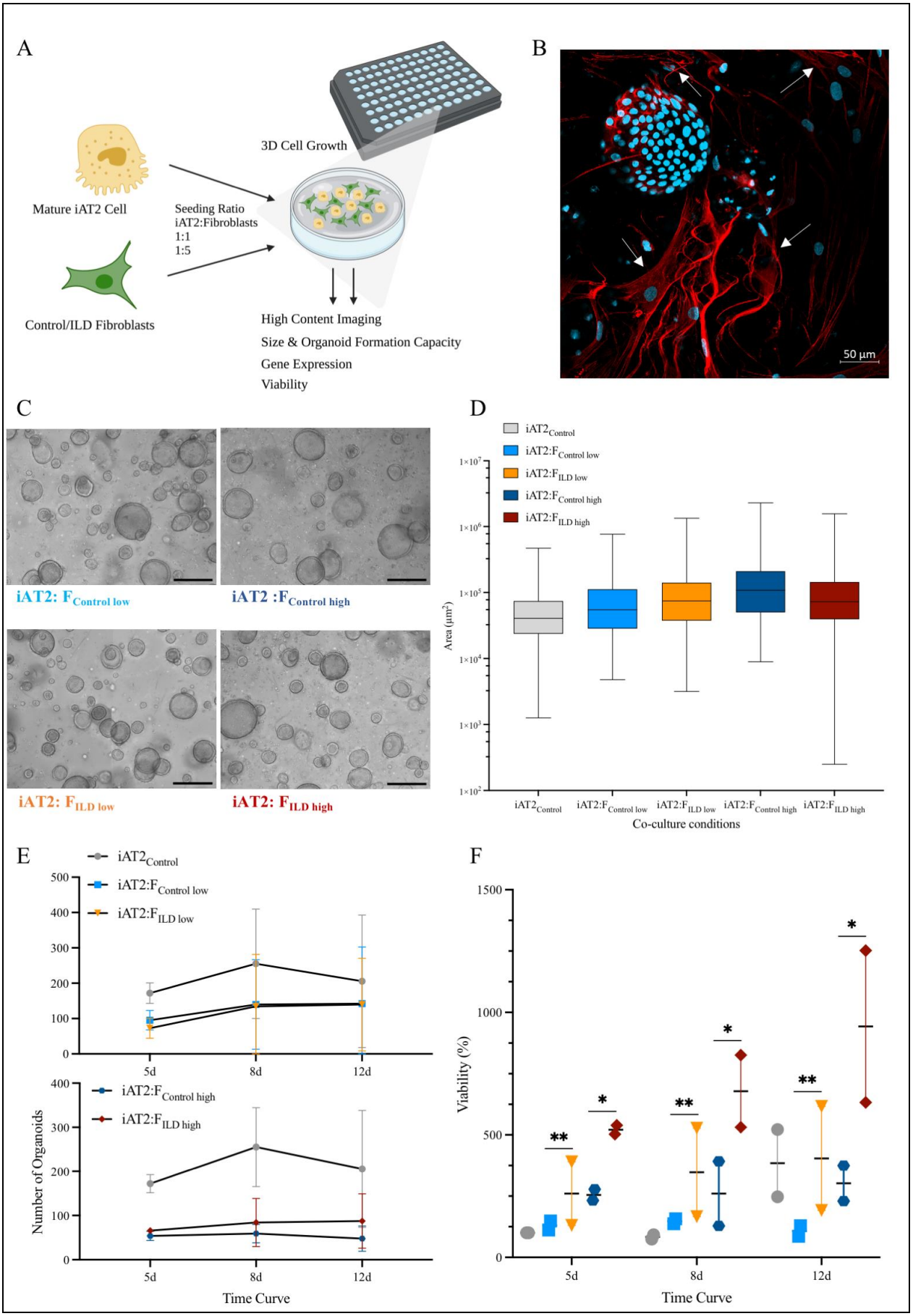
A
3D Cell Growth
Mature iAT2 Cell
Seeding Ratio
iAT2:Fibroblasts
1:1
1:5
Control/ILD Fibroblasts
High Content Imaging
Size & Organoid Formation Capacity
Gene Expression
Viability
B
50 µm
C
iAT2: F Control low
iAT2 :F Control high
iAT2: F ILD low
iAT2: F ILD high
D
iAT2 Control
iAT2:F Control low
iAT2:F ILD low
iAT2:F Control high
iAT2:F ILD high
Area (µm²)
Co-culture conditions
E
iAT2 Control
iAT2:F Control low
iAT2:F ILD low
iAT2:F Control high
iAT2:F ILD high
Number of Organoids
Time Curve
F
Viability (%)
Time Curve

265

Figure 1. **3D co-culture of iAT2 and primary fibroblasts**
(A) Schematic workflow of the 3D co-culture model of iAT2s with IMR-90 control or ILD fibroblasts at different seeding densities in a matrix dome analyzed for size, organoid morphology and metabolic activity. (B) Immunofluorescence of 3D co-culture of iAT2s and ILD fibroblasts at day 12 (α-SMA: red, DAPI: cyan). (C) Representative maximum intensity projections from high-content images of different co-culture conditions showing iAT2s growing with human fibroblasts for 12 days. Scale bar, 500 µm. (D) Box plots indicate size (μm^2) of organoids in co-culture at day 12. N = 3. (E) Number of formed organoids in co-cultures at day 12, N = 3. (F) Metabolic activity of co-cultured organoids estimated by WST-1 assay at 5, 8 and 12 days. Results are represented relative to co-cultures with IMR-90 control fibroblasts at each time point. N = 2. Statistics: unpaired t-Test.

3.2 ILD signaling leads to aberrant epithelial gene expression changes

In order to relate the observed changes in morphology, organoid formation capacity and metabolic activity (Figure 1) to changes in gene expression levels, we measured critical markers of stem cell function and epithelial differentiation in co-cultured organoids.

Indicating changes in (stem) cell function and epithelial injury, we showed decreased expression of the alveolar stem cell marker *SFTPC* in the presence of ILD lung fibroblasts in both seeding conditions (Figure 2A and Supplementary Figure 2). In line with this, *Keratin 8* (*KRT8*) expression levels were downregulated under the impact of ILD primary fibroblasts, additionally indicating the limited capacity for alveolar regeneration (Figure 2A and Supplementary Figure 2). The distal epithelial marker *Integrin Subunit Beta 6* (*ITGB6*) as well as *Bone Morphogenetic Protein 4* (*BMP4*) showed increased transcription in the disease context with $F_{ILD\ high}$ only (Figure 2B and Supplementary Figure 2). Genes associated with regulation of extracellular matrix formation and remodeling including *Collagen 1A1* (*Col1A1*), *N-Cadherin* (*CDH2*) and *Vimentin* (*VIM*) showed increased expression in co-culture models of iAT2s with high seeding ratio of ILD fibroblasts, indicating EMT and not in $F_{ILD\ low}$ (Figure 2B and Supplementary Figure 2).

Expression levels for *Matrix Metallopeptidase 7* (*MMP7*), one of the best studied peripheral blood biomarkers for matrix remodeling in IPF, showed an increase in mRNA expression when comparing $F_{ILD\ high}$ with the respective IMR-90 control (Figure 2B and Supplementary Figure 2). Relative expression of these genes in ILD and control fibroblast monocultures, is predominantly lower than in co-cultures with iAT2s, pointing towards their expression from stimulated epithelium (Supplementary Figure 3).

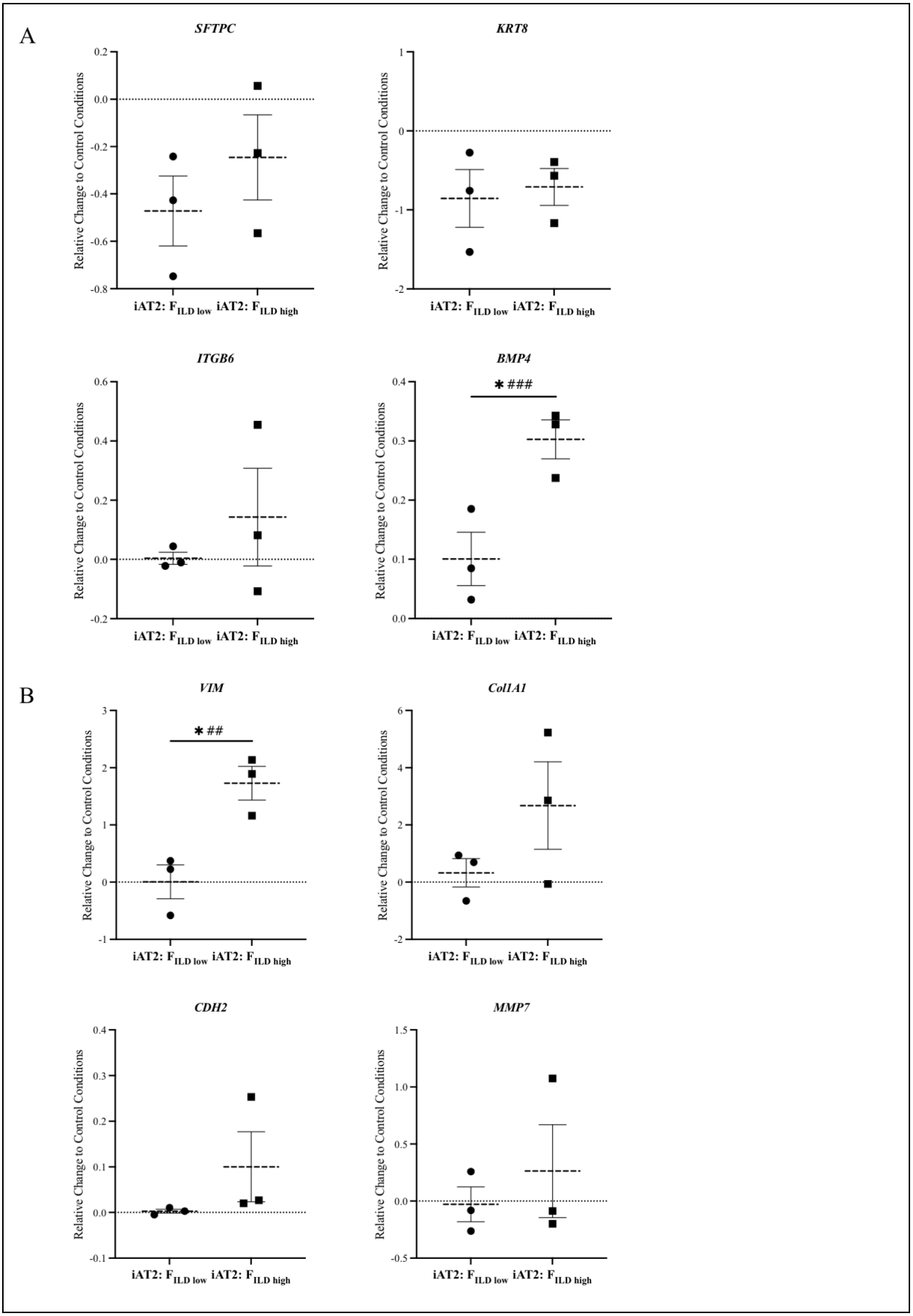
A
SFTPC
KRT8
ITGB6
BMP4
* ###
B
VIM
* ##
Col1A1
CDH2
MMP7
Relative Change to Control Conditions
iAT2: F ILD low
iAT2: F ILD high

296

Figure 2. **Gene expression in ILD and IMR-90 control organoid co-cultures**
(A) Fold change of gene expression relative to control conditions for epithelial and stem cell markers in co-culture conditions of iAT2s with ILD fibroblasts in two seeding densities ($F_{ILD\ high}$ and $F_{ILD\ low}$). N = 3, unpaired t-Test, ### highly significant compared to HK (Supplementary Figure 2). (B) Fold change of gene expression relative to control conditions for markers associated with aberrant differentiation in co-culture conditions of iAT2s with ILD fibroblasts in two seeding densities ($F_{ILD\ high}$ and $F_{ILD\ low}$). N = 3, unpaired t-Test, ## highly significant compared to HK (Supplementary Figure 2).

3.3 ILD fibroblast secretome reveals proinflammatory signaling converging on IL11 stimulating epithelial remodeling

To characterize fibroblast driven communication resulting in gene expression and phenotypical changes in the alveolar epithelium in ILD, supernatants of ILD and non-CLD fibroblast were subjected to mass spectrometry (MS).
MS analysis detected 2625 expressed proteins resulting in 47 significantly upregulated and 55 significantly downregulated proteins compared to non-CLD controls (Supplementary Table 3 and 4) (Figure 3A). The top 15 differentially regulated proteins are listed in Supplementary Table 1 and 2. Upregulated proteins widely belong to the C-X-C motif chemokine family (CXCL1, CXCL3, and CXCL8) indicating pro-inflammatory signaling, leucocyte attraction and tissue remodeling (Kortekaas et al., 2022; Mukaida, 2003; Ng et al., 2020; Strikoudis et al., 2019). Furthermore, significantly regulated proteins support a pro-inflammation response indicating pro-fibrotic signaling, IL13-related responses (IL13RA) and IL11 at the center of the signaling circuit. We found upregulated proteins involved in cell differentiation and growth included Gap Junction protein connexin 43 (GJA1), and Pregnancy Specific Beta-1-Glyoprotein 4 (PSG4), involved in ECM and tissue remodeling as well as modulators of WNT signaling (SFRP4).
Pathway enrichment analysis of significantly upregulated proteins classified the responses as cytokine activity, chemokine-mediated signaling pathway as well as TNF-signaling pathway. Furthermore, cellular/response to chemokines, IL17 signaling pathways and neutrophil chemotaxis were found, indicative of a strong inflammatory response. The prominent center identified by ClueGo analysis are proteins associated with rheumatoid arthritis, a disease often associated with development of lung fibrosis surrounded by the abundant presence of inflammatory chemokines (Figure 3B).
Most downregulated proteins are involved in ECM production, assembly or reorganization as well as coordination of myofibroblast differentiation (PDGFRL). Furthermore, the complement and coagulation cascade pathways are significantly down-regulated in ILD secretome (Figure 3C).

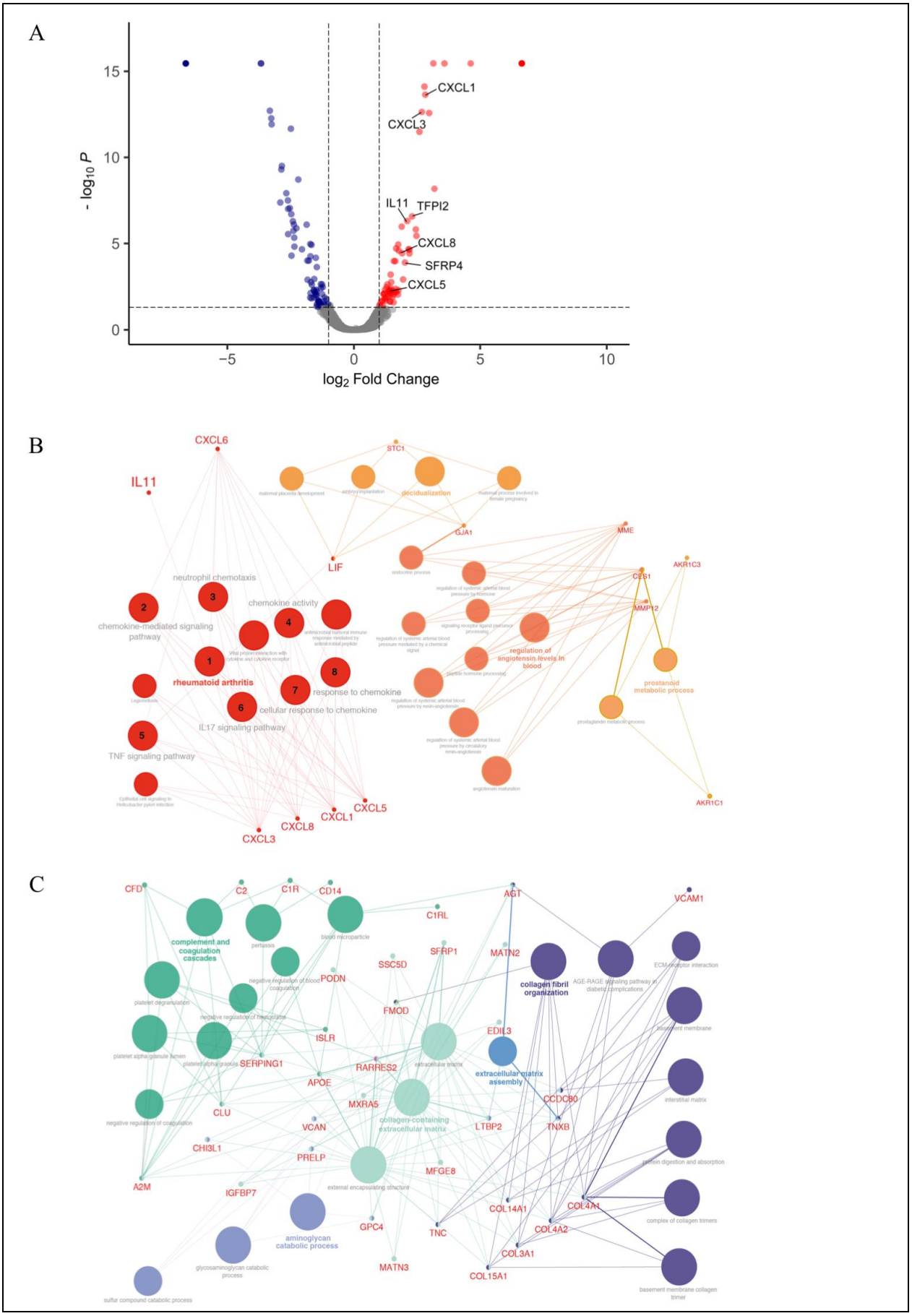
A
- log10 P
log2 Fold Change
CXCL1
CXCL3
IL11
TFPI2
CXCL8
SFRP4
CXCL5
B
CXCL6
IL11
STC1
decidualization
GJA1
MME
LIF
AKR1C3
CES1
MMP12
neutrophil chemotaxis
chemokine activity
chemokine-mediated signaling pathway
rheumatoid arthritis
response to chemokine
cellular response to chemokine
IL17 signaling pathway
TNF signaling pathway
regulation of angiotensin levels in blood
prostanoid metabolic process
AKR1C1
CXCL5
CXCL1
CXCL8
CXCL3
C
CFD
C2
C1R
CD14
AGT
VCAM1
C1RL
complement and coagulation cascades
SFRP1
MATN2
SSC5D
PODN
collagen fibril organization
FMOD
EDIL3
ISLR
SERPING1
RARRES2
extracellular matrix assembly
APOE
CCDC80
MXRA5
CLU
VCAN
LTBP2
TNXB
CHI3L1
PRELP
MFGE8
A2M
IGFBP7
COL14A1
COL4A1
GPC4
TNC
COL4A2
aminoglycan catabolic process
COL3A1
MATN3
COL15A1

328

Figure 3. **Secreted ligands of MS secretom analysis**
(A) Volcano plot visualizing significantly regulated proteins (47 up, 55 down) found in secretome analysis of ILD or non-CLD control fibroblasts by MS. Data showing the $\log_2$ fold change against the adjusted P value [log10]. Significant upregulated proteins are depicted in red and significant downregulated proteins in blue. (total: 102 significantly changing proteins with FDR < 0.05). Pathway enrichment and protein interaction network of (B) upregulated proteins and (C) downregulated proteins using the Cytoscaspe plugin ClueGo. The following ontologies were used: KEGG, molecular functions and biological processes. The connectivity of the pathways is described by functional nodes and edges that are shared between proteins with a kappa score of 0.4. Only enriched pathways are visualized and the node size indicates the p-value (p-value ≤ 0.05). Proteins from the same pathway share the same node color and the bold fonts indicate the most important functional pathways that define the names of each group.
Enriched Pathways: 1. rheumatoid arthritis, 2. chemokine-mediated signaling pathway, 3. neutrophil chemotaxis, 4. chemokine activity, 5. TNF signaling pathway, 6. IL17 signaling pathway, 7. cellular response to chemokine, 8. response to chemokine.

3.4 IL11 acts as a driver for aberrant signatures in hiPSC-derived alveolospheres

Pathway enrichment analysis indicated rheumatoid arthritis as central hallmark according to identified secreted protein profiles. IL11 acts as master regulator in RA, orchestrating the CXCL dominated inflammatory response. IL11 with its bi-inflammatory signaling capacity has been described to be involved in a range of chronic inflammatory lung diseases, including asthma, COPD and IPF (Cui et al., 2022). Furthermore, it has gathered attention as potential therapeutic targeting (Ng et al., 2019). Therefore, we chose IL11 for modified organoid experiments to validate its functional relevance as critical player in the ILD fibroblast secretome. After stimulation of the alveolospheres with IL11 in dose-response experiments ($Dose_{low}$ = 0.5 ng/mL), $Dose_{high}$ = 5 ng/mL), (Figure 4B - D) recapitulated the results observed epithelial-fibroblasts co-cultures. We demonstrated that mature alveolospheres in a 3D matrix under the impact of IL11 from day 7 - 14 of culture show morphologic changes with increased organoid size (Figure 4C (ii) and (iii)) and reduced organoid formation capacity (Figure 4C (iii) and 4D) when compared to untreated non-CLD fibroblasts. Furthermore, metabolic activity (WST-1) of IL11 treated iAT2s increased strongly over the treatment period (Figure 4D), again in line with the results obtained in co-culture experiments (section 3.1). Treatment of growing alveolosphere monocultures with a dose of 20 ng/mL IL11 led to the formation of large organoids followed by apoptosis within 5 days of culture.

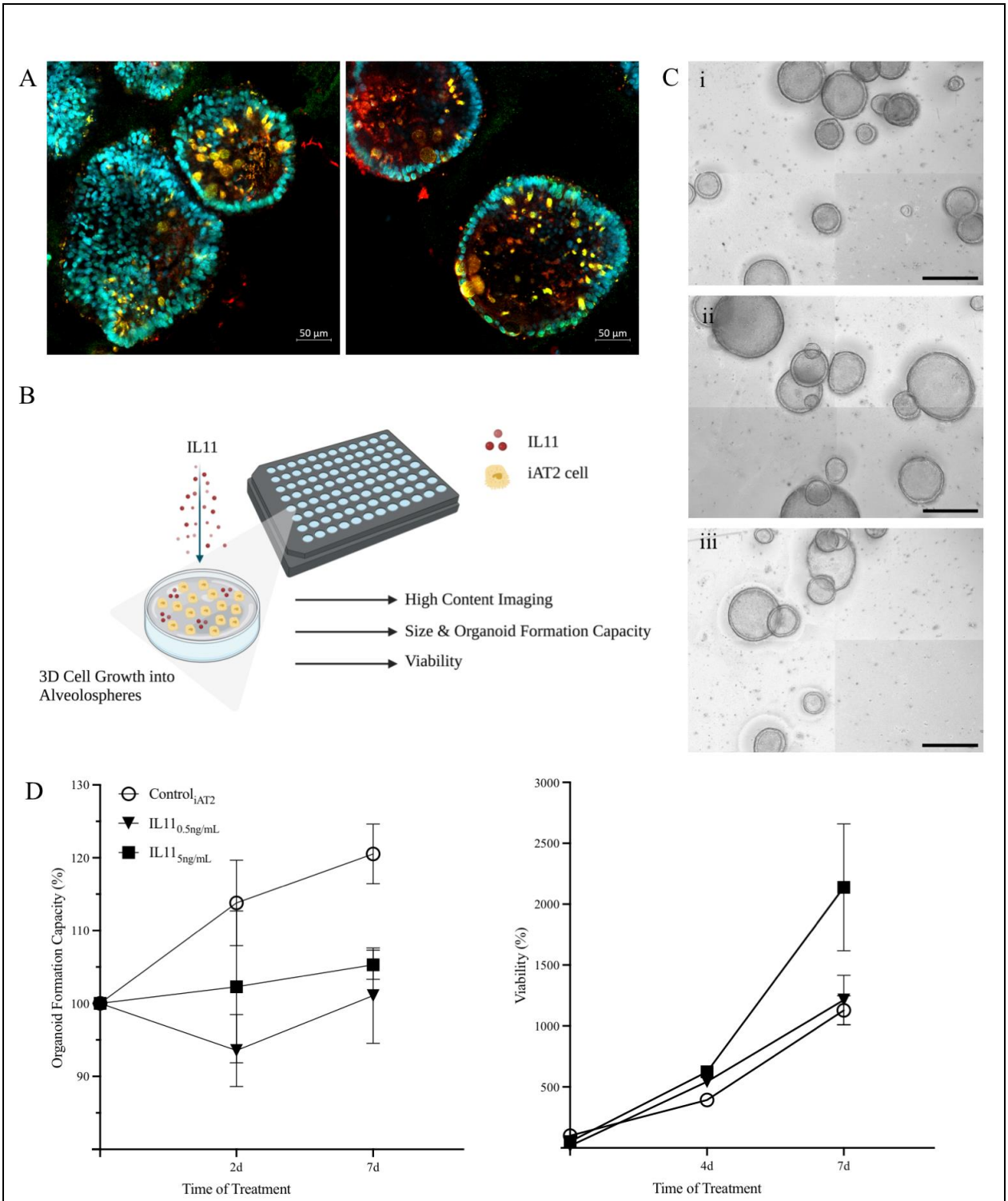
A
50 µm
50 µm
B
IL11
IL11
iAT2 cell
High Content Imaging
Size & Organoid Formation Capacity
Viability
3D Cell Growth into
Alveolospheres
C
i
ii
iii
D
Control$_{iAT2}$
IL11$_{0.5ng/mL}$
IL11$_{5ng/mL}$
Organoid Formation Capacity (%)
130
120
110
100
90
2d
7d
Time of Treatment
Viability (%)
3000
2500
2000
1500
1000
500
4d
7d
Time of Treatment

359

Figure 4. **Cytokine treatment of iAT2s in a 3D culture**
(A) Immunofluorescence of alveolosphere monoculture at day 14 (SFTPC: red, NKX2.1: green, DAPI: cyan). (B) Schematic workflow of organoid treatment starting at day 7 of culture. Treatment with IL11 (0.5 ng/mL or 5 ng/mL) occurred every 48 h for additional 7 days before analyzing alveolospheres. (C) Representative maximum intensity projections from high-content images of (i) untreated monocultured alveolospheres, (ii) 0.5 ng/mL or (iii) 5 ng/mL. Scale bar, 500 µm. (D) Data represent organoid formation capacity and metabolic activity estimated by WST-1 assay in IL11 treated alveolospheres.

4 Discussion

In ILD, sustained inflammation and scarring of the gas exchange area ultimately results in organ failure. Excessive deposition of ECM and remodeling of the lung scaffold along with inflammation-driven epithelial damage and dedifferentiation is widely transmitted by the misguided interaction of fibroblasts and epithelial cells (Lewis et al., 2018). Therefore, improved understanding of the mesenchymal-to-epithelial crosstalk remains a centerpiece in finding new avenues to monitor and treat ILD. However, the signaling factors and their involvement to ILD pathogenesis is still unclear.

This study aimed at deciphering functionally relevant candidates with a key role in mesenchymal-to-epithelial crosstalk to identify potential targets for future therapeutic strategies. By using a sensitive human iPSC-derived alveolar organoid co-culture model and secretome analysis of ILD fibroblasts, we highlighted the functional importance of cytokine-driven aberrant epithelial differentiation upon fibroblast signaling. In our unbiased proteomic approach, we identified IL11 in the top 15 regulated proteins as key regulator of the observed, fibroblast–driven immune signaling. Its central role in chronic inflammatory lung diseases and its function as key mediator of pro-fibrotic mesenchymal-epithelial crosstalk supported our observations together with demonstrating its functional relevance our human alveolosphere model (Cook & Schafer, 2020; Ng et al., 2020; Ng et al., 2019).

In our *in vitro* co-culture approach, primary human pulmonary fibroblasts and iAT2s formed lung organoids. The 3D matrix recapitulates tissue characteristics of the distal lung in contrast to 2D plastic culture conditions (Figure 1). Primary human fibroblasts, both ILD and IMR-90 control cells, correlating with seeding numbers but in a disease-independent manner, reduced organoid number and led to an increase in organoid size after 12 days of co-culture. These findings indicate that the presence of either, ILD or control (IMR-90) fibroblasts changes the microenvironment of iAT2s, thereby impacting on organoid growth. As studies indicated the easily-induced activation of primary lung fibroblasts resembling disease characteristics (Kathiriya et al., 2022), these findings might explain the uniform response of iAT2 organoids to fibroblasts independent of disease status but likely related to fibroblast activation per se.

The ILD-induced, significant increase in metabolic activity, however, was provoked by high-seeding ratios of diseased fibroblasts (Figure 1F), indicating a potential role of ILD lung fibroblasts on epithelial cell metabolic reprogramming potentially indicative of epithelial dedifferentiation, and possibly EMT (Kalluri, 2009; Kalluri & Weinberg, 2009; Wang et al., 2020). The loss of epithelial stem cell characteristics is also supported by the decrease in SFTPC expression in ILD co-cultures (Adams et al., 2020; Katzen & Beers, 2020; Kortekaas et al., 2021). *SFTPC* expression is sensitive to epithelial inflammation and injury and can be restored after regeneration as has been observed by e.g., negative regulation of SFTPC in Sars-CoV-2 infected alveolar organoids (Mou, 2021). Differentiation of AT2s is necessary for regeneration of injured alveoli and drive them into expressing transient basaloid features marked by *Keratin 5* (*KRT5*) expression. The elucidation of this identity change is critical as the amount of alveolar *KRT5*$^{+}$ aberrant basaloid cells directly correlates with mortality in pulmonary fibrosis (Kathiriya et al., 2022; Khan et al., 2022; Ng et al., 2022).

An important marker in the transdifferentiation of AT2 to AT1 phenotype during epithelial regeneration is *KRT8* (Ng et al., 2022; Strunz et al., 2020). Downregulation of *KRT8* marks the stage of pre-AT1 like cells in a murine bleomycin lung injury model, also associated with the expression of EMT markers. Furthermore, this particular state also shows the expression of pro-fibrogenic proteins

including *ITGB6* (Strunz et al., 2020). In our study, *ITGB6* expression is upregulated specifically in the ILD co-cultures and potentially reflects on EMT processes in lung organoids together with the downregulation of *KRT8*. Supportive of these findings are the elevated relative expression of *BMP4* and *MMP7* in the lung organoids cultured with ILD fibroblasts which have been shown to be master regulators of EMT in pulmonary fibrosis (Molloy et al., 2008). *MMP7* is involved in regulating lung injury and one of the most important biomarkers in peripheral blood in the diagnosis of idiopathic pulmonary fibrosis (Adams et al., 2020; Bauer et al., 2017). Co-culture of alveolospheres with ILD fibroblasts also specifically changed the expression of genes involved in ECM biosynthesis. The increased transcription of *Col1A1*, *VIM* and *CDH2* implies partly that fibroblasts increase matrix production or deposition when cultured with diseased fibroblasts (Adams et al., 2020; Katzen & Beers, 2020). These genes show elevated expression in fibrotic lungs, it supports the disease crosstalk in the ILD co-culture model and the resulted. (Ng et al., 2022) In contrast, it has been shown recently that primary alveolar epithelial cells undergo aberrant basal transdifferentiation stimulated by IPF fibroblasts co-culture (Kathiriya et al., 2022). The basaloid cells show increased ECM protein as well as *BMP4* and *ITGB6* expression as detected in our model. The overlap in transcriptional profiles could therefore indicate an aberrant basaloid state of the hiPSC-derived lung organoids after ILD fibroblast co-culture, detrimental in the initiation of pulmonary fibrosis.

To understand mesenchymal-to-epithelial crosstalk leading to the changes in organoid phenotype and gene expression, we analyzed the supernatant of ILD or control fibroblasts in an unbiased approach by mass spectrometry (Strieter et al., 2007). Cytokines that belong to the C-X-C motif family dominate the upregulated proteins in the secretome. These signaling molecules act on the CXCR1 and CXCR2 receptor, as well as regulate the expression of cytokines from the interleukin family, central to the pathogenesis of fibrotic and inflammatory lung diseases such as IPF and acute respiratory distress syndrome (ARDS) (Kortekaas et al., 2022; Mukaida, 2003; Ng et al., 2020; Strikoudis et al., 2019). The majority of the differentially regulated proteins are proinflammatory cytokines that primarily act on neutrophil and monocyte or lymphocyte recruitment (CXCL 1, 3, 5, 8). The proinflammatory response is complemented by the regulation of proteins that induce cellular senescence and activate soluble or matrix bound TGF-ß such as the Pregnancy-Specific Glycoprotein (PSG) family, PSG 4, 5, 6 or induce a hypercoagulable environment (TFPI2). SFRP4 directly inhibits WNT signaling modulating cell growth and differentiation particularly involved in the transdifferentiation of AT2 towards AT1 (Abdelwahab et al., 2019). At the same time, WNT serum levels are discussed as a potential biomarker for EMT and severity of lung fibrosis. These factors, particularly WNT modulation and TGF-ß solubilization, might explain the phenotypical change in organoid number and size and support gene expression levels that indicate epithelial transdifferentiation into aberrant basaloid cells or a fibroblast-like phenotype when co-cultured with ILD fibroblasts.

We detected IL11, centrally orchestrating the ILD protein profile as observed by pathway enrichment, among the top 15 regulated candidates in the secretome of ILD primary fibroblasts. IL11 is highly upregulated in pro-inflammatory fibroblasts as extracted from IPF lungs. The cytokine belongs to the IL6 family and is induced by TGF-ß stimulation and other proinflammatory mediators (IL1β, IL17, IL22, reactive oxygen species (ROS)). It can either activate fibroblasts to differentiate into myofibroblasts in an autocrine fashion through ERK/SMAD canonical signaling for pro-fibrotic protein expression (COL1A1, ACTA2). Furthermore, it stimulates epithelial cells (paracrine loop) through activating ERK signaling cascades inducing cellular senescence, EMT and chronic dysfunction as well as impaired regeneration (Ng et al., 2020). In our co-culture models we observed gene expression patterns and phenotypical changes that indicate both the autocrine and paracrine features of IL11 signaling including EMT, stem cell dysfunction (phenotypical changes Figure 1, epithelial gene expression Figure 2) as well as collagen upregulation (mesenchyme associated genes Figure 2), also shown by (Ng et al., 2020). Similar as observed for iAT2 co-cultures with different seeding densities of ILD fibroblasts (Figure 1), direct treatment of alveolosphere monocultures with

IL11 caused a dose dependent increase in their metabolic activity (Figure 4) associated with elevated mesenchymal markers and decreases in AT2 stemness and identity (Figure 2). High levels of IL11 (20 ng/mL) even induced apoptotic cell death (data not shown) supporting the strong induction of senescence and disturbance of stem cell function in alveolar organoids (Kortekaas et al., 2022). These results are in line with modeling Hermansky-Pudlak syndrome-associated interstitial pneumonia (HPSIP), a disease with high similarity to IPF, in iPSC-derived lung organoids shown by Strikoudis et al. 2019. IL11 alone induced fibrotic changes in healthy alveolar organoids and knock-out of IL11 expression in diseases organoids reversed organoid fibrosis (Strikoudis et al., 2019). Moreover, IL11 exposure impacts on the progenitor function that characterizes AT2s, thereby likely suppressing the formation of mature AT2s as described by Kortekaas and colleagues (Kortekaas et al., 2022; Kortekaas et al., 2021).

Our results strongly support the central role of IL11 signaling, amongst the top regulated cytokines in the ILD fibroblast secretome, in early events of ILD initiation. IL11 strongly influences the intricate crosstalk between activated (myo)fibroblasts and damaged epithelial cells which is decisive in the progression of pulmonary fibrosis in ILD. Furthermore, we demonstrate the functional potential of lung organoid co-culture models derived from hiPSCs displaying aberrant dedifferentiation and basaloid-prone signatures resulting from mesenchyme-to-epithelial driven failure (Adams et al., 2020; Habermann et al., 2020). IL11 induced alveolar differentiation may mislead regeneration by destroying the homeostasis in the alveolar space and result in AT2 dysfunction and offers a valuable and promising therapeutic target (Lin et al., 2022).

Conflict of Interest

The authors declare that the research was conducted in the absence of any commercial or financial relationships that could be construed as a potential conflict of interest.

Author Contributions

M.T. Kastlmeier, A. Hilgendorff and C. Voss conceived and planned the experiments. M.T. Kastlmeier and E. Gonzalez Rodriguez carried out the experiments. M.T. Kastlmeier, E. Gonzalez Rodriguez, P. Cabanis, E. M. Guenther contributed to sample preparation. A-C. König and S. Hauck performed the mass spectrometry analysis. M.T. Kastlmeier, C. Voss, T. Stoeger, A-C. König, S. Hauck and A. Hilgendorff contributed to the interpretation of the results. M.T. Kastlmeier and C. Voss. took the lead in writing the manuscript. All authors provided critical feedback and helped shape the research, analysis and manuscript.

Funding

This project was supported by the Research Training Group GRK2338 of the DFG, LMU Munich. Further funding was received by the German Center of Lung Research (DZL) and Helmholtz Munich.

Acknowledgments

We wish to thank the Kotton Lab especially Prof. Darrell Kotton by providing the hiPSC cell line. We are grateful to David Kutschke for technical assistance. We gratefully acknowledge the provision of human biomaterial (primary human fibroblasts) and clinical data from the CPC-M bioArchive and its partners at the Asklepios Biobank Gauting, the LMU Hospital and the Ludwig-Maximilians-Universität München. We thank the patients and their families for their support. We thank Zeynep Ertüz for creating the graphical abstract. We thank the Research Unit Analytical Pathology (AAP, Helmholtz Center Munich) with Dr. Ulrike Buchholz and Dr. Annette Feuchtinger for their assistance during confocal imaging. We thank Benoite Champon and Dr. Minodora Brimpari for their help with the FACS cell sorting at the MACSQuant Tyto Cell Sorter.

5 References

Abdelwahab, E. M. M., Rapp, J., Feller, D., Csongei, V., Pal, S., Bartis, D., Thickett, D. R., & Pongracz, J. E. (2019). Wnt signaling regulates trans-differentiation of stem cell like type 2 alveolar epithelial cells to type 1 epithelial cells. *Respiratory Research*, *20*(1), 204. https://doi.org/10.1186/s12931-019-1176-x

Adams, T. S., Schupp, J. C., Poli, S., Ayaub, E. A., Neumark, N., Ahangari, F., Chu, S. G., Raby, B. A., DeIuliis, G., Januszyk, M., Duan, Q., Arnett, H. A., Siddiqui, A., Washko, G. R., Homer, R., Yan, X., Rosas, I. O., & Kaminski, N. (2020). Single-cell RNA-seq reveals ectopic and aberrant lung-resident cell populations in idiopathic pulmonary fibrosis. *Science Advances*, *6*(28), eaba1983. https://doi.org/doi:10.1126/sciadv.aba1983

Bauer, Y., White, E. S., de Bernard, S., Cornelisse, P., Leconte, I., Morganti, A., Roux, S., & Nayler, O. (2017). MMP-7 is a predictive biomarker of disease progression in patients with idiopathic pulmonary fibrosis. *ERJ Open Res*, *3*(1). https://doi.org/10.1183/23120541.00074-2016

Bindea, G., Mlecnik, B., Hackl, H., Charoentong, P., Tosolini, M., Kirilovsky, A., Fridman, W. H., Pagès, F., Trajanoski, Z., & Galon, J. (2009). ClueGO: a Cytoscape plug-in to decipher functionally grouped gene ontology and pathway annotation networks. *Bioinformatics*, *25*(8), 1091-1093. https://doi.org/10.1093/bioinformatics/btp101

Cook, S. A., & Schafer, S. (2020). Hiding in Plain Sight: Interleukin-11 Emerges as a Master Regulator of Fibrosis, Tissue Integrity, and Stromal Inflammation. *Annu Rev Med*, *71*, 263-276. https://doi.org/10.1146/annurev-med-041818-011649

Cui, F., Sun, Y., Xie, J., Li, D., Wu, M., Song, L., Hu, Y., & Tian, Y. (2022). Air pollutants, genetic susceptibility and risk of incident idiopathic pulmonary fibrosis. *European Respiratory Journal*, 2200777. https://doi.org/10.1183/13993003.00777-2022

Glasser, S. W., Hardie, W. D., & Hagood, J. S. (2010). Pathogenesis of Interstitial Lung Disease in Children and Adults. *Pediatr Allergy Immunol Pulmonol*, *23*(1), 9-14. https://doi.org/10.1089/ped.2010.0004

Habermann, A. C., Gutierrez, A. J., Bui, L. T., Yahn, S. L., Winters, N. I., Calvi, C. L., Peter, L., Chung, M. I., Taylor, C. J., Jetter, C., Raju, L., Roberson, J., Ding, G., Wood, L., Sucre, J. M. S., Richmond, B. W., Serezani, A. P., McDonnell, W. J., Mallal, S. B., . . . Kropski, J. A. (2020). Single-cell RNA sequencing reveals profibrotic roles of distinct epithelial and mesenchymal lineages in pulmonary fibrosis. *Sci Adv*, *6*(28), eaba1972. https://doi.org/10.1126/sciadv.aba1972

Hawkins, F., Kramer, P., Jacob, A., Driver, I., Thomas, D. C., McCauley, K. B., Skvir, N., Crane, A. M., Kurmann, A. A., Hollenberg, A. N., Nguyen, S., Wong, B. G., Khalil, A. S., Huang, S. X., Guttentag, S., Rock, J. R., Shannon, J. M., Davis, B. R., & Kotton, D. N. (2017). Prospective isolation of NKX2-1-expressing human lung progenitors derived from pluripotent stem cells. *J Clin Invest*, *127*(6), 2277-2294. https://doi.org/10.1172/jci89950

Heinzelmann, K., Lehmann, M., Gerckens, M., Noskovičová, N., Frankenberger, M., Lindner, M., Hatz, R., Behr, J., Hilgendorff, A., Königshoff, M., & Eickelberg, O. (2018). Cell-surface phenotyping identifies CD36 and CD97 as novel markers of fibroblast quiescence in lung fibrosis. *Am J Physiol Lung Cell Mol Physiol*, *315*(5), L682-l696. https://doi.org/10.1152/ajplung.00439.2017

Hogan, M. Z. N. a. B. L. M. (2021). Lung Stem Cells in Development, Health and Disease. In *ERS monograph*.

Jacob, A., Morley, M., Hawkins, F., McCauley, K. B., Jean, J. C., Heins, H., Na, C.-L., Weaver, T. E., Vedaie, M., Hurley, K., Hinds, A., Russo, S. J., Kook, S., Zacharias, W., Ochs, M.,

Traber, K., Quinton, L. J., Crane, A., Davis, B. R., . . . Kotton, D. N. (2017). Differentiation of Human Pluripotent Stem Cells into Functional Lung Alveolar Epithelial Cells. *Cell stem cell*, *21*(4), 472-488.e410. https://doi.org/10.1016/j.stem.2017.08.014

Jacob, A., Vedaie, M., Roberts, D. A., Thomas, D. C., Villacorta-Martin, C., Alysandratos, K.-D., Hawkins, F., & Kotton, D. N. (2019). Derivation of self-renewing lung alveolar epithelial type II cells from human pluripotent stem cells. *Nature protocols*, *14*(12), 3303-3332. https://doi.org/10.1038/s41596-019-0220-0

Kalluri, R. (2009). EMT: When epithelial cells decide to become mesenchymal-like cells. *The Journal of Clinical Investigation*, *119*(6), 1417-1419. https://doi.org/10.1172/JCI39675

Kalluri, R., & Weinberg, R. A. (2009). The basics of epithelial-mesenchymal transition. *The Journal of Clinical Investigation*, *119*(6), 1420-1428. https://doi.org/10.1172/JCI39104

Kastlmeier, M. T., Guenther, E. M., Stoeger, T., & Voss, C. (2022). Lung Organoids for Hazard Assessment of Nanomaterials. *International Journal of Molecular Sciences*, *23*(24), 15666. https://www.mdpi.com/1422-0067/23/24/15666

Kathiriya, J. J., Wang, C., Zhou, M., Brumwell, A., Cassandras, M., Le Saux, C. J., Cohen, M., Alysandratos, K.-D., Wang, B., Wolters, P., Matthay, M., Kotton, D. N., Chapman, H. A., & Peng, T. (2022). Human alveolar type 2 epithelium transdifferentiates into metaplastic KRT5+ basal cells. *Nature Cell Biology*, *24*(1), 10-23. https://doi.org/10.1038/s41556-021-00809-4

Katzen, J., & Beers, M. F. (2020). Contributions of alveolar epithelial cell quality control to pulmonary fibrosis. *The Journal of Clinical Investigation*, *130*(10), 5088-5099. https://doi.org/10.1172/JCI139519

Khan, P., Roux, J., Blumer, S., Knudsen, L., Jonigk, D., Kuehnel, M. P., Tamm, M., & Hostettler, K. E. (2022). Alveolar Basal Cells Differentiate towards Secretory Epithelial- and Aberrant Basaloid-like Cells In Vitro. *Cells*, *11*(11). https://doi.org/10.3390/cells11111820

Kim, K. K., Sheppard, D., & Chapman, H. A. (2018). TGF-β1 Signaling and Tissue Fibrosis. *Cold Spring Harb Perspect Biol*, *10*(4). https://doi.org/10.1101/cshperspect.a022293

Kong, J., Wen, S., Cao, W., Yue, P., Xu, X., Zhang, Y., Luo, L., Chen, T., Li, L., Wang, F., Tao, J., Zhou, G., Luo, S., Liu, A., & Bao, F. (2021). Lung organoids, useful tools for investigating epithelial repair after lung injury. *Stem Cell Research & Therapy*, *12*(1), 95. https://doi.org/10.1186/s13287-021-02172-5

Kortekaas, R., Geillinger-Kästle, K., Borghuis, T., Belharch, K., Webster, M., Timens, W., Burgess, J., & Gosens, R. (2022). IL-11 disrupts alveolar epithelial progenitor function. In: bioRxiv.

Kortekaas, R. K., Burgess, J. K., Webster, M., & Gosens, R. (2021). IL11 negatively impacts adult lung alveolar organoid formation. *ERJ Open Research*, *7*(suppl 6), 81. https://doi.org/10.1183/23120541.Lsc-2021.81

Lederer, D. J., & Martinez, F. J. (2018). Idiopathic Pulmonary Fibrosis. *N Engl J Med*, *378*(19), 1811-1823. https://doi.org/10.1056/NEJMra1705751

Lewis, K. J. R., Hall, J. K., Kiyotake, E. A., Christensen, T., Balasubramaniam, V., & Anseth, K. S. (2018). Epithelial-mesenchymal crosstalk influences cellular behavior in a 3D alveolus-fibroblast model system. *Biomaterials*, *155*, 124-134. https://doi.org/10.1016/j.biomaterials.2017.11.008

Lin, C. R., Bahmed, K., & Kosmider, B. (2022). Impaired Alveolar Re-Epithelialization in Pulmonary Emphysema. *Cells*, *11*(13). https://doi.org/10.3390/cells11132055

Molloy, E. L., Adams, A., Moore, J. B., Masterson, J. C., Madrigal-Estebas, L., Mahon, B. P., & O'Dea, S. (2008). BMP4 induces an epithelial-mesenchymal transition-like response in adult airway epithelial cells. *Growth Factors*, *26*(1), 12-22. https://doi.org/10.1080/08977190801987166

Mou, H. (2021). Induced Pluripotent Stem Cell-derived Alveolar Type II Heterogeneity: Revealed by SFTPC Expression. *American journal of respiratory cell and molecular biology*, *65*(4), 345-346. https://doi.org/10.1165/rcmb.2021-0242ED

Mukaida, N. (2003). Pathophysiological roles of interleukin-8/CXCL8 in pulmonary diseases. *American Journal of Physiology-Lung Cellular and Molecular Physiology*, *284*(4), L566-L577. https://doi.org/10.1152/ajplung.00233.2002

Navarro, P., Trevisan-Herraz, M., Bonzon-Kulichenko, E., Núñez, E., Martínez-Acedo, P., Pérez-Hernández, D., Jorge, I., Mesa, R., Calvo, E., Carrascal, M., Hernáez, M. L., García, F., Bárcena, J. A., Ashman, K., Abian, J., Gil, C., Redondo, J. M., & Vázquez, J. (2014). General statistical framework for quantitative proteomics by stable isotope labeling. *J Proteome Res*, *13*(3), 1234-1247. https://doi.org/10.1021/pr4006958

Ng, B., Cook, S. A., & Schafer, S. (2020). Interleukin-11 signaling underlies fibrosis, parenchymal dysfunction, and chronic inflammation of the airway. *Exp Mol Med*, *52*(12), 1871-1878. https://doi.org/10.1038/s12276-020-00531-5

Ng, B., Dong, J., D'Agostino, G., Viswanathan, S., Widjaja, A. A., Lim, W. W., Ko, N. S. J., Tan, J., Chothani, S. P., Huang, B., Xie, C., Pua, C. J., Chacko, A. M., Guimarães-Camboa, N., Evans, S. M., Byrne, A. J., Maher, T. M., Liang, J., Jiang, D., . . . Cook, S. A. (2019). Interleukin-11 is a therapeutic target in idiopathic pulmonary fibrosis. *Sci Transl Med*, *11*(511). https://doi.org/10.1126/scitranslmed.aaw1237

Ng, B., Huang, K. Y., Pua, C. J., Lim, W.-W., Kuthubudeen, F., Hii, A. A., Viswanathan, S., Petretto, E., & Cook, S. A. (2022). Interleukin-11 causes alveolar type 2 cell dysfunction and prevents alveolar regeneration. *bioRxiv*, 2022.2011.2011.516109. https://doi.org/10.1101/2022.11.11.516109

Nikolić, M. Z., Sun, D., & Rawlins, E. L. (2018). Human lung development: recent progress and new challenges. *Development*, *145*(16). https://doi.org/10.1242/dev.163485

O'Dwyer, D. N., Ashley, S. L., & Moore, B. B. (2016). Influences of innate immunity, autophagy, and fibroblast activation in the pathogenesis of lung fibrosis. *American Journal of Physiology-Lung Cellular and Molecular Physiology*, *311*(3), L590-L601. https://doi.org/10.1152/ajplung.00221.2016

Strieter, R. M., Gomperts, B. N., & Keane, M. P. (2007). The role of CXC chemokines in pulmonary fibrosis. *J Clin Invest*, *117*(3), 549-556. https://doi.org/10.1172/jci30562

Strikoudis, A., Cieślak, A., Loffredo, L., Chen, Y. W., Patel, N., Saqi, A., Lederer, D. J., & Snoeck, H. W. (2019). Modeling of Fibrotic Lung Disease Using 3D Organoids Derived from Human Pluripotent Stem Cells. *Cell Rep*, *27*(12), 3709-3723.e3705. https://doi.org/10.1016/j.celrep.2019.05.077

Strunz, M., Simon, L. M., Ansari, M., Kathiriya, J. J., Angelidis, I., Mayr, C. H., Tsidiridis, G., Lange, M., Mattner, L. F., Yee, M., Ogar, P., Sengupta, A., Kukhtevich, I., Schneider, R., Zhao, Z., Voss, C., Stoeger, T., Neumann, J. H. L., Hilgendorff, A., . . . Schiller, H. B. (2020). Alveolar regeneration through a Krt8+ transitional stem cell state that persists in human lung fibrosis. *Nature Communications*, *11*(1), 3559. https://doi.org/10.1038/s41467-020-17358-3

Wang, Y., Dong, C., & Zhou, B. P. (2020). Metabolic reprogram associated with epithelial-mesenchymal transition in tumor progression and metastasis. *Genes & Diseases*, *7*(2), 172-184. https://doi.org/https://doi.org/10.1016/j.gendis.2019.09.012

Yao, L., Zhou, Y., Li, J., Wickens, L., Conforti, F., Rattu, A., Ibrahim, F. M., Alzetani, A., Marshall, B. G., Fletcher, S. V., Hancock, D., Wallis, T., Downward, J., Ewing, R. M., Richeldi, L., Skipp, P., Davies, D. E., Jones, M. G., & Wang, Y. (2021). Bidirectional epithelial-mesenchymal crosstalk provides self-sustaining profibrotic signals in pulmonary fibrosis. *J Biol Chem*, *297*(3), 101096. https://doi.org/10.1016/j.jbc.2021.101096

Supplementary Material

1 Supplementary Figures and Tables

1.1 Supplementary Tables

Supplementary Table 1. **Antibodies and dilutions for immunofluorescence staining**

Antibody	**Manufacturer**	**Host Species**	**Isotype**	**Reactivity**	**Clonality**	**Dilution**
ALB	R&D Systems Cat# MAB1455 Clone# 188835	mouse	IgG2a	human, mouse, rat	monoclonal	1:50
α- SMA	Abcam Cat# ab124964 Lot# GR303485-6	rabbit	NA	human, mouse, rat	monoclonal	1:200
CPM	Fujifilm Wako Chemicals Cat# 014-27501	mouse	IgG2b	human	monoclonal	1:200
NKX2.1	Invitrogen Cat# MA5-13961 Clone# 8G7G3/1	mouse	IgG1 κ	human, mouse, rat	monoclonal	1:50
Pro SP-C	Millipore Cat # AB3786 Lot# 2464523	rabbit	IgG	human, mouse, rat	polyclonal	1:200
Alexa Flour 488	Invitrogen	anti-mouse	IgG1			1:500
Alexa Flour 647	Invitrogen	anti-rabbit				1:500
DAPI	Sigma					1:1000

Supplementary Table 2. **Primer sequences for qPCR**

Gene symbol	**Forward**	**Reverse**
ß-Actin	CAATGTGGCCGAGGACTTTG	CATTCTCCTTAGAGAGAAGTGG
BMP4	TAGCAAGAGTGCCGTCATTCC	GCGCTCAGGATACTCAAGACC

CDH2	TCAGGCGTCTGTAGAGGCTT	ATGCACATCCTTCGATAAGACTG
Col1A1	TACAGAACGGCCTCAGGTACCA	ACAGATCACGTCATCGCACAAC
HRPT	AAGAGCTATTGTAATGACCAGT	CAAAGTCTGCATTGTTTTGC
ITGB6	TCCATCTGGAGTTGGCGAAAG	TCTGTCTGCCTACACTGAGAG
KRT8	CAGAAGTCCTACAAGGTGTCCA	CTCTGGTTGACCGTAACTGCG
MMP7	GAGTGAGCTACAGTGGGAACA	CTATGACGCGGGAGTTTAACAT
SPC	CACCTGAAACGCCTTCTTATCG	TTTCTGGCTCATGTGGAGACC
VIM	GACGCCATCAACACCGAGTT	CTTTGTCGTTGGTTAGCTGGT

Supplementary Table 3. **List of upregulated proteins compared $F_{Control}$ vs. F_{ILD} identified by mass spectrometry**

Protein FDR confidence	**Accession**	**Unique peptides**	**Gene symbol**	**Description**	**Abundance ratio**	**Abundance ratio P-value**	**Abundance ratio adj. P-value**
High	Q68BL8	2	OLFML2B	Olfactomedin-like protein 2B	100,00	0,0000	0,0000
High	Q9C0H2	3	TTYH3	Protein tweety homolog 3	100,00	0,0000	0,0000
High	Q96FV2	2	SCRN2	Secernin-2	100,00	0,0000	0,0000
High	Q9UHX1	3	PUF60	Poly(U)-binding-splicing factor PUF60	100,00	0,0000	0,0000
High	Q16630	2	CPSF6	Cleavage and polyadenylation specificity factor subunit 6	100,00	0,0000	0,0000
High	Q00888	8	PSG4	Pregnancy-specific beta-1-glycoprotein 4	8,81	0,0000	0,0000
High	P17302	3	GJA1	Gap junction alpha-1 protein	7,85	0,0000	0,0000
High	P09341	2	CXCL1	Growth-regulated alpha protein	7,06	0,0000	0,0000
High	P19876	3	CXCL3	C-X-C motif chemokine 3	6,42	0,0000	0,0000
High	Q14956	2	GPNMB	Transmembrane glycoprotein NMB	6,02	0,0000	0,0000

High	P48307	11	TFPI2	Tissue factor pathway inhibitor 2	4,92	0,0000	0,0000
High	Q14627	3	IL13RA2	Interleukin-13 receptor subunit alpha-2	4,46	0,0000	0,0000
High	P20809	3	IL11	Interleukin-11	4,31	0,0000	0,0000
High	Q6FHJ7	2	SFRP4	Secreted frizzled-related protein 4	4,05	0,0000	0,0001
High	P10145	2	CXCL8	Interleukin-8	3,75	0,0000	0,0000

Supplementary Table 4. **List of downregulated proteins compared $F_{Control}$ vs. F_{ILD} identified by mass spectrometry**

Protein FDR confidence	**Accession**	**Unique peptides**	**Gene symbol**	**Description**	**Abundance ratio**	**Abundance ratio P-value**	**Abundance ratio adj. P-value**
High	Q15198	5	PDGFRL	Platelet-derived growth factor receptor-like protein	0,49	0,0025	0,0325
High	P10321	4	HLA-C	HLA class I histocompatibility antigen, C alpha chain	0,47	0,0012	0,0172
High	P22352	8	GPX3	Glutathione peroxidase 3	0,43	0,0002	0,0034
High	Q9NZP8	7	C1RL	Complement C1r subcomponent-like protein	0,42	0,0001	0,0024
High	P24821	87	TNC	Tenascin	0,42	0,0043	0,0500
High	Q9NR99	36	MXRA5	Matrix-remodeling-associated protein 5	0,42	0,0041	0,0488
High	Q13822	29	ENPP2	Ectonucleotide pyrophosphatase/phosphodiesterase family member 2	0,42	0,0041	0,0485
High	Q76M96	25	CCDC80	Coiled-coil domain-containing protein 80	0,41	0,0039	0,0473
High	O43854	20	EDIL3	EGF-like repeat and discoidin I-like domain-containing protein 3	0,41	0,0038	0,0457
High	Q9NRN5	13	OLFML3	Olfactomedin-like protein 3	0,41	0,0038	0,0458
High	P02461	61	COL3A1	Collagen alpha-1(III) chain	0,41	0,0035	0,0434
High	P62906	7	RPL10A	60S ribosomal protein L10a	0,41	0,0031	0,0391

High	P00746	15	CFD	Complement factor D	0,41	0,0031	0,0391
High	O00339	17	MATN2	Matrilin-2	0,40	0,0002	0,0039
High	O15232	11	MATN3	Matrilin-3	0,40	0,0001	0,0023

1.2 Supplementary Figures

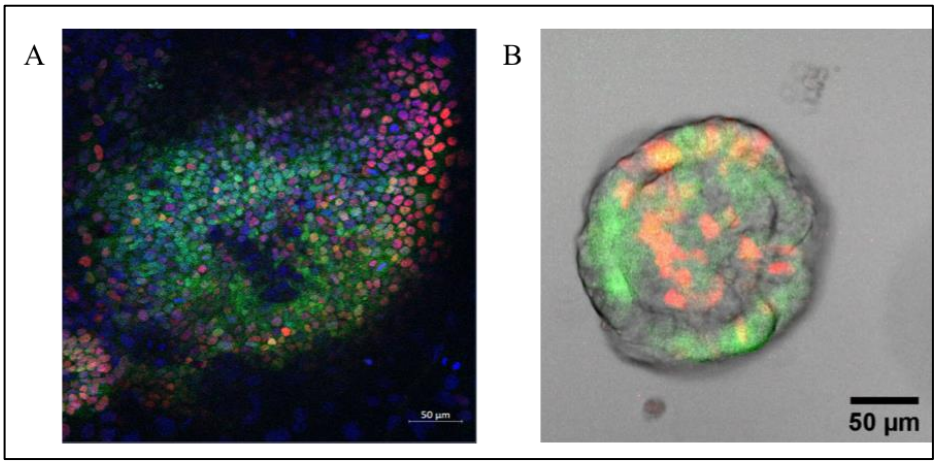

Supplementary Figure 1. **iAT2 containing alveolospheres obtained from hiPSCs by chemically directed lung differentiation**

(A) Immunofluorescence of day 14 lung progenitors from directed lung differentiation (ALB: red, NKX2.1: green, DAPI: cyan). (B) iAT2 alveolosphere at day 44 of differentiation (BU3NGST cell line; NKX2.1^{GFP}, SFTPC^{tdTomato}).

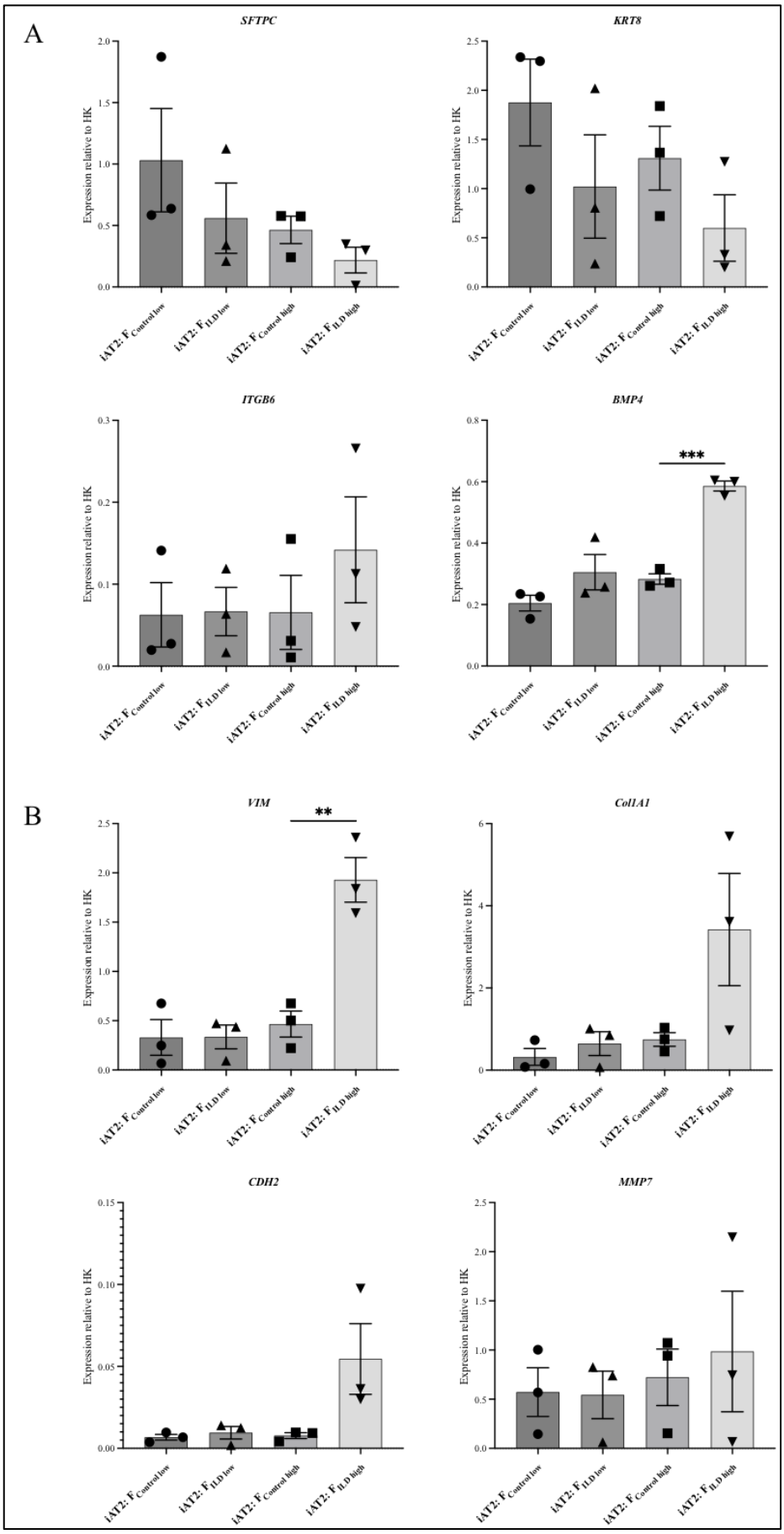
A
SFTPC
KRT8
ITGB6
BMP4
***
B
VIM
**
Col1A1
CDH2
MMP7
Expression relative to HK
iAT2: F Control low
iAT2: F ILD low
iAT2: F Control high
iAT2: F ILD high

Supplementary Figure 2. **Relative gene expression of 3D co-cultures to HK**

(A) Fold change of gene expression relative to HK (average of ß-Actin and HRPT) for epithelial and stem cell markers in co-culture conditions of iAT2s with IMR-90 control and ILD fibroblasts in in two seeding densities (F_{high} and F_{low}). N = 3, unpaired t-Test between F_{high} and F_{low}. (B) Fold change of gene expression relative to HK (average of ß-Actin and HRPT) for markers associated with aberrant differentiation in co-culture conditions of iAT2s with IMR-90 control and ILD fibroblasts in two seeding densities (F_{high} and F_{low}). N = 3, unpaired t-Test between F_{high} and F_{low}.

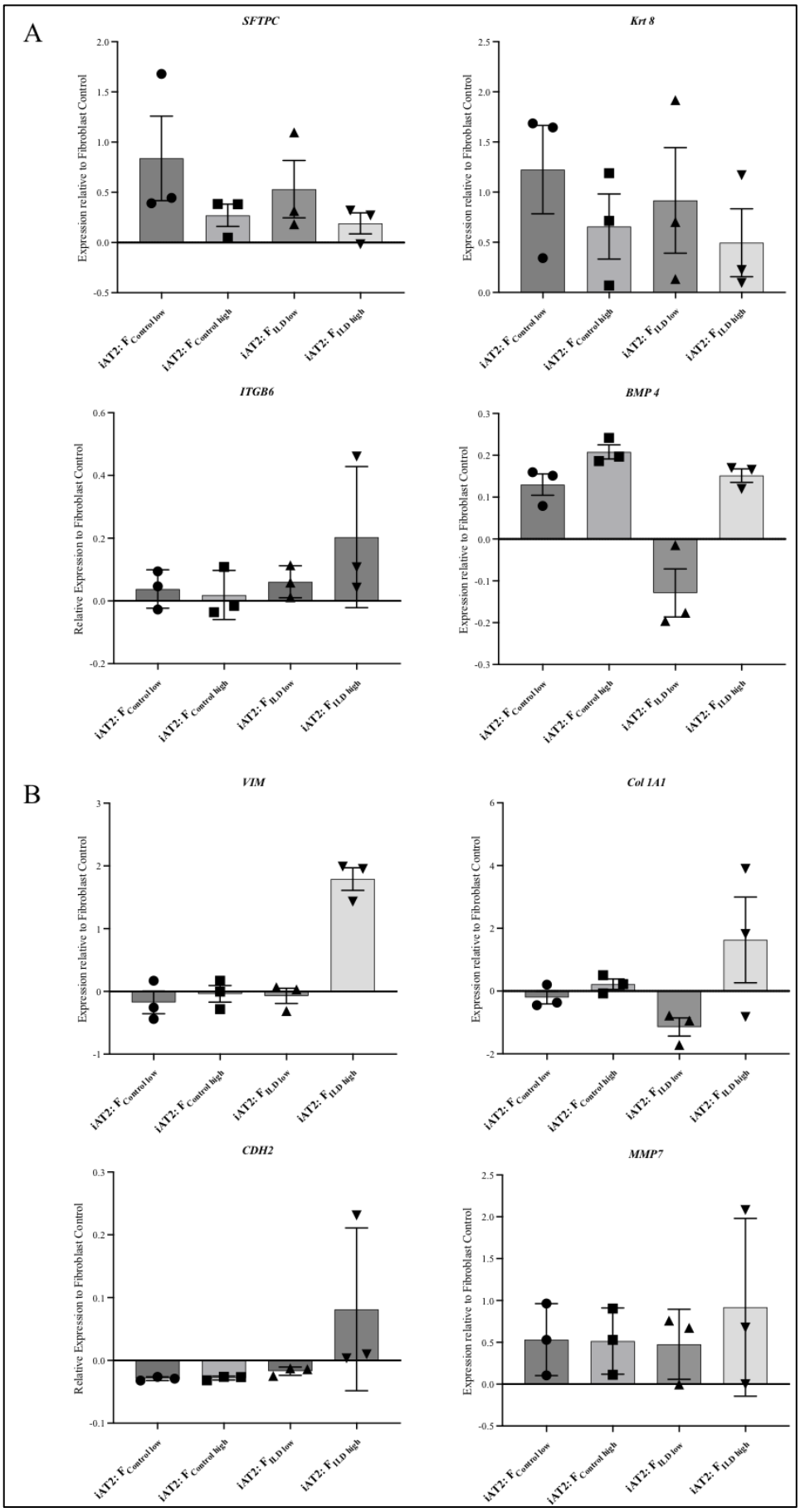
A
SFTPC
Expression relative to Fibroblast Control
Krt 8
Expression relative to Fibroblast Control
ITGB6
Relative Expression to Fibroblast Control
BMP 4
Expression relative to Fibroblast Control
B
VIM
Expression relative to Fibroblast Control
Col 1A1
Expression relative to Fibroblast Control
CDH2
Relative Expression to Fibroblast Control
MMP7
Expression relative to Fibroblast Control
iAT2: F Control low
iAT2: F Control high
iAT2: F ILD low
iAT2: F ILD high

Supplementary Figure 3. **Gene expression of 3D co-cultures relative to control fibroblasts**

(A) Fold change of gene expression relative to monocultured IMR-90 control fibroblasts for epithelial and stem cell markers in co-culture conditions of iAT2s with IMR-90 control and ILD fibroblasts in in two seeding densities (F_{high} and F_{low}). N = 3, ordinary one-way ANOVA. (B) Fold change of gene expression relative to monocultured IMR-90 control fibroblasts for markers associated with aberrant differentiation in co-culture conditions of iAT2s with IMR-90 control and ILD fibroblasts in two seeding densities (F_{high} and F_{low}). N = 3, ordinary one-way ANOVA.